Molecular Polarity in Tropomyosin-Troponin T Co-Crystals

Donna Cabral-Lilly,* Larry S. Tobacman,# John P. Mehegan,# and Carolyn Cohen*
*Rosenstiel Basic Medical Sciences Research Center, Brandeis University, Waltham, Massachusetts 02254-9110, and #Department of Internal Medicine, University of Iowa College of Medicine, Iowa City, Iowa 52242-0001 USA

ABSTRACT New features of the structure and interactions of troponin T and tropomyosin have been revealed by electron microscopy of so-called double-diamond co-crystals. These co-crystals were formed using rabbit α_2 tropomyosin complexed with troponin T from either skeletal or cardiac muscle, which have different lengths in the amino-terminal region, as well as a bacterially expressed skeletal muscle troponin T fragment of 190 residues that lacks the amino-terminal region. Differences in the images of the co-crystals have allowed us to establish the polarities of both the troponin T subunit and tropomyosin in the projected lattice. Moreover, in agreement with their sequences, the amino-terminal region of a bovine cardiac muscle troponin T isoform appears to be longer than that from the rabbit skeletal muscle troponin T isoform and to span more of the amino terminus of tropomyosin at the head-to-tail filament joints. Images of crystals tilted relative to the electron beam also reveal the supercoiling of the tropomyosin filaments in this lattice. Based on these results, a three-dimensional model of the double-diamond lattice has been constructed.

INTRODUCTION

Troponin T (TnT; M_r 33,000) is a key component of the regulatory switch in vertebrate skeletal and cardiac muscle. TnT, together with troponins I (TnI; M_r 24,000) and C (TnC; M_r 18,000) forms a complex that binds at intervals of 400 Å along the tropomyosin filament (Ebashi and Endo, 1968; Flicker et al., 1982; Cohen et al., 1972). TnT is an elongated molecule that binds directly to tropomyosin filaments to anchor the regulatory complex to the thin filament (Mak and Smillie, 1981; Flicker et al., 1982; Ishii and Lehrer, 1991; Dahiya et al., 1994). The amino-terminal portion of TnT spans the tropomyosin filament head-to-tail joint, and the rest of the subunit extends approximately 180 Å along the tropomyosin molecule (White et al., 1987; Mak et al., 1983). The amino-terminal portion of TnT increases the cooperativity of myosin binding to the thin filament (Schaertl et al., 1995). TnC and TnI form a globular complex that binds to the carboxyl-terminal region of TnT.

There are many different isoforms of TnT (for review see Bandman, 1992), some of which have been sequenced (for example, see Leszyk et al., 1987; Gahlmann et al., 1987; Mesnard et al., 1993; Pearlstone et al., 1986). Different isoforms are also developmentally regulated (Briggs and Schachat, 1993; Cooper and Ordahl, 1985) and specific for skeletal or cardiac tissue (Breitbart et al., 1985; Anderson et al., 1991). The most variable region among TnT isoforms is the amino-terminal portion, here defined as the sequence preceding the conserved Pro-47 of rabbit fast skeletal muscle TnT (Pearlstone et al., 1977). Among major isoforms, this region can be as short as 31 amino acids in rat fast skeletal muscle (Breitbart et al., 1985) or as long as 89 amino acids in newborn rabbit heart (Grieg et al., 1994) and in chicken embryo heart (Cooper and Ordahl, 1985). Its heterogeneity is increased by alternative splicing of the 5′ portions of cardiac muscle, fast skeletal muscle, and slow skeletal muscle TnT gene transcripts, which also undergo splicing of other regions. Despite the resultant TnT isoform variability, cardiac TnTs are consistently larger than those from skeletal muscle due to a greater length of the amino-terminal region. For example, the amino-terminal regions of TnT isoforms in cardiac versus skeletal muscle are 87 vs. 49–54 amino acids in fetal rat and 77 vs. 25–45 amino acids in adult rat (Jin and Lin, 1989; Breitbart et al., 1985). Similar patterns are found in rabbit (Grieg et al., 1994; Briggs and Schachat, 1993) and chicken (Cooper and Ordahl, 1985; Wilkinson et al., 1984; Smillie et al., 1988). Recently, the adult cardiac muscle isoform of TnT was recognized as an important serum marker in the diagnosis of several types of myocardial injury in humans (for review see Mair et al., 1992), and a highly sensitive enzyme immunoassay for cardiac TnT has been developed for use in coronary heart disease diagnosis and prognosis (Katus et al., 1992). There is little information, however, about possible structural differences among TnT isoforms and whether these are important in regulatory function.

TnT has not yet been crystallized, but this subunit readily forms a co-crystal with tropomyosin, called the double-diamond mesh, that is especially suitable for electron microscopy (Cohen et al., 1972; Margossian and Cohen, 1973; Carr et al., 1988). All of the crystal forms of native tropomyosin are composed of polar filaments of molecules bonded head-to-tail with a short overlap, and the cross-connections in the lattice are related to specific interactions of the tropomyosin molecules (Phillips et al., 1986; Whitby et al., 1992; Xie et al., 1994). In the double-diamond mesh, however, it is primarily the interactions of the TnT subunits that determine the form of the lattice. In this co-crystal,

Received for publication 21 October 1996 and in final form 30 June 1997.
Address reprint requests to Dr. Carolyn Cohen, Rosenstiel Basic Medical Sciences Research Center, Brandeis University, Waltham, MA 02254-9110. Tel.: 617-736-2466; Fax: 617-736-2419; E-mail:ccohen@binah.cc.brandeis.edu.

D. Cabral-Lilly's present address: The Liposome Co., Princeton, NJ.

0006-3495/97/10/1763/08 $2.00

pairs of tropomyosin filaments are linked at one end by pairs of interacting TnT subunits. The crossovers in the lattice (which appear as bright nodes in electron micrographs of negatively stained co-crystals) are separated by ~100 Å and ~300 Å, giving a mesh of alternating large and small diamonds (Fig. 1 *A*). The lattice in projection has *cmm* plane group symmetry (Cohen et al., 1972) with unit cell dimensions of ~726 Å and ~324 Å for *a* and *b*, respectively (Fig. 1 *A*, inset). Because of this symmetry, in the three-dimensional lattice the tropomyosin filaments interact with the TnT subunits facing each other. By using certain tissue-specific isoforms of TnT as well as an expressed truncated form of this subunit, we have established the polarity of TnT binding to tropomyosin, as well as additional features of the molecular interactions in the lattice.

MATERIALS AND METHODS

Protein isolation and crystallization

α_2-Tropomyosin was purified from frozen rabbit hearts as described by Phillips et al. (1979). Rabbit skeletal muscle TnT (TnT259) was isolated from rabbit psoas muscle according to Greaser and Gergely (1973). This TnT259 was used without separating different TnT isoforms. The major isoform of bovine cardiac TnT (TnT284) was isolated as described by Tobacman and Lee (1987). A fragment of rat skeletal muscle TnT (TnT_{trunc}) missing the amino terminus region was expressed in *E. coli* DE3 cells and

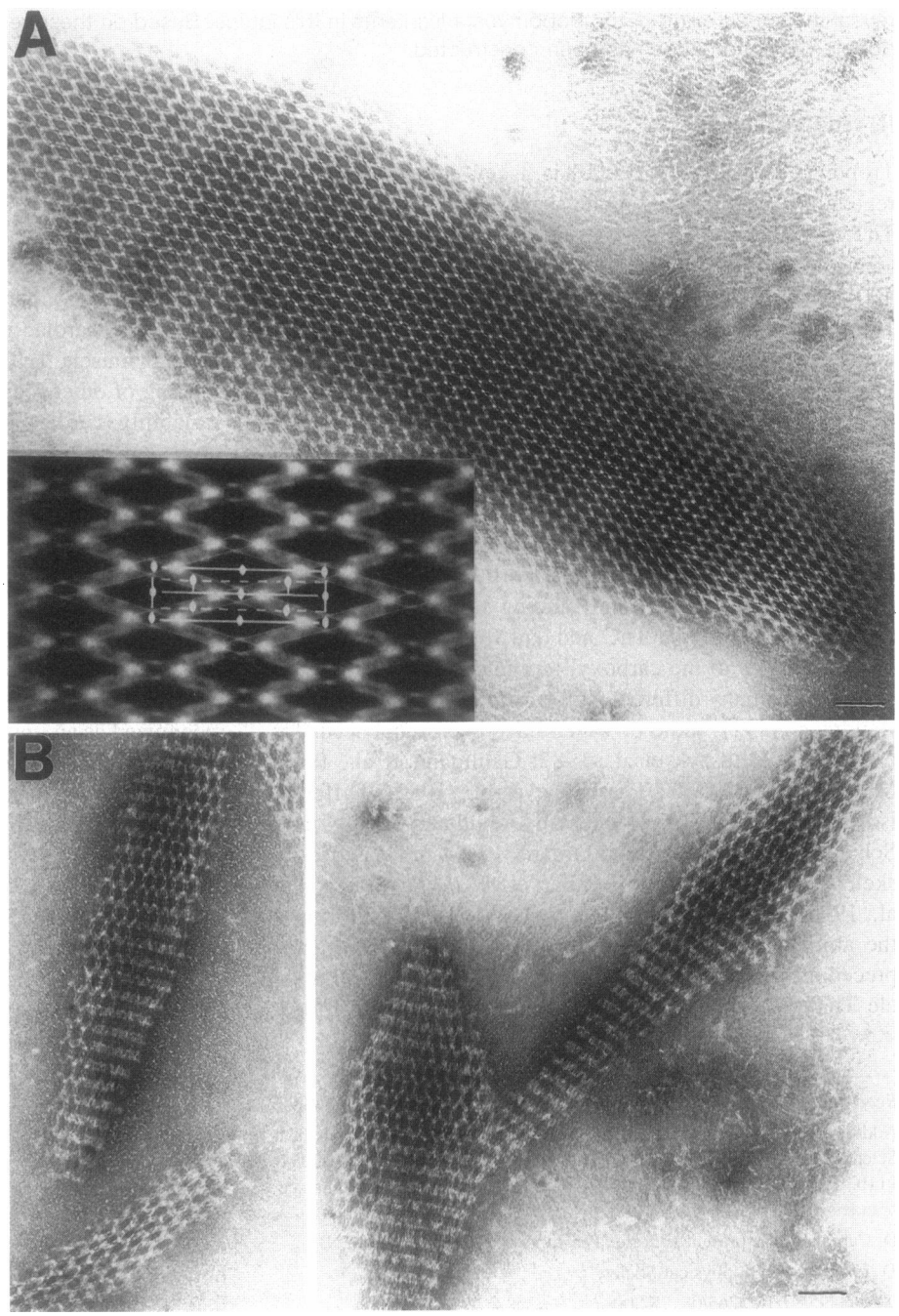

FIGURE 1 Electron micrographs of double diamond co-crystals of tropomyosin-TnT specimens in negative stain. Protein appears as white on a black background. The open-mesh pattern in the images collapses at one end into the double-ladder tactoid observed by others for these crystals (Cohen et al., 1972; Carr et al., 1988). (*A*) Image of a double diamond crystal of rabbit α_2-tropomyosin and rabbit skeletal TnT negatively stained with uranyl acetate. Bar, 100 nm. The inset shows a noise-filtered image of a selected portion enlarged approximately three times. An area of the lattice outlining the double-diamond pattern is shown (*thin white lines*) with one unit cell (*thick white lines*) and associated symmetry elements. The projection (viewed down *c*) has *cmm* plane group symmetry with a = ~726 Å and b = ~324 Å. (*B*) Electron micrographs of representative tropomyosin-TnT_{trunc} co-crystals. Bar, 100 nm.

purified as described in Hill et al. (1992). TnT_{trunc} is 97% homologous to residues 70–259 of rabbit skeletal muscle TnT.

Double-diamond crystals of tropomyosin-TnT259 or tropomyosin-TnT_{trunc} were made by first mixing equimolar ratios of tropomyosin and TnT in 0.6 M KCl, 50 mM Tris, pH 8.0, at a total protein concentration of 1.5 mg/ml. The protein solution was then dialyzed at 4°C against 0.1 M sodium acetate, 0.05 M ammonium sulfate, pH 5.6. Tropomyosin and TnT284 were co-crystallized by dialysis against 0.1 M ammonium sulfate, 0.01 M sodium acetate, pH 5.6. In all cases, a fine white precipitate formed overnight.

Electron microscopy and image processing

Electron micrographs of negatively stained double diamonds were recorded at an electron dose of approximately 10 $e^-/Å^2$ at a nominal magnification of ×48,000 and 3000–7000 Å underfocus. Areas of micrographs showing clear double diamonds were digitized using an Eikonix model 1412 scanner at 25 μm raster corresponding to 5.4 Å/pixel. Noise-filtered images were produced according to Carr et al. (1988) using a 1.5-pixel radius for the final two-dimensional Fourier mask.

Crystals of tropomyosin-TnT259 and tropomyosin-TnT284 were also preserved unstained in vitreous ice and viewed at −172°C as described previously (Cabral-Lilly et al., 1991). Electron micrographs were recorded at 5000 Å defocus and at electron doses of <10 $e^-/Å^2$. Selected micrographs were digitized using an Eikonics imaging system at a raster step of 5.4 Å/pixel. The average image size was 900 × 900 pixels (~100 unit cells). For images of unstained crystals viewed in projection, lattice distortions were corrected and structure factors extracted from computed transforms of the unbent crystals according to Henderson et al. (1986). The structure factors were not corrected for the effects of the contrast transfer function. It should be noted, however, that the first zero of the transfer function fell outside the range of useful data so that corrections were not necessary for the phase component of the structure factors. The phase origin was refined and the *cmm* plane group symmetry of this projection was imposed (Cohen et al., 1972). The mean nonweighted phase residuals upon imposing *cmm* symmetry were 32.4° and 32.6° for the tropomyosin-TnT284 and tropomyosin-TnT259 co-crystals, respectively.

Similarities and differences between the crystals formed with the two TnT isoforms were explored as follows. The resolution for each structure factor set was filtered to 20 Å, and images produced for 11 or 7 data sets for the cardiac and skeletal TnT co-crystals, respectively. The images were then normalized and average maps computed for each of the two groups (Cabral-Lilly et al., 1991). A difference image was computed by subtracting the skeletal average image from the cardiac average. Finally, a significance map was computed by applying the Student's *t*-test on a pixel by pixel basis (Trachtenberg et al., 1987), using 15° of freedom and a 95% cutoff. The question being asked is whether the cardiac and skeletal averages are statistically different. Statistically significant regions are represented by either white or black pixels in the significance image; gray regions are not statistically different. Dark regions in the difference map correspond to additional protein present in the cardiac average and give rise to black regions in the significance map. White regions correspond to a deficiency of protein in the cardiac average relative to the skeletal average.

RESULTS AND DISCUSSION

A previously unsolved question about the double-diamond lattice is the polarity of both the TnT and tropomyosin molecules. It had not been possible to deduce the polarity as one end of the TnT subunit is obscured in the lattice, although an orientation has been proposed based on indirect evidence (Carr et al., 1988). In this study, the polarity of TnT in the lattice was determined directly by using double-diamond co-crystals containing a bacterially expressed rat skeletal muscle carboxyl-terminal fragment of TnT (TnT_{trunc}). This fragment contains residues 70–259, numbered according to the rabbit protein sequence (Pearlstone et al., 1977). Although the co-crystals formed with TnT_{trunc} are smaller than those with the native subunit and tend to collapse at the ends, the key crystal contact at the acute vertex of the large diamond is maintained despite the absence of a large portion of the TnT amino terminus (Fig. 1 *B*). Moreover, when TnC, which binds to the carboxyl-terminal region of TnT, is mixed with tropomyosin and TnT before crystallization, the double-diamond lattice is not formed; instead, the Bailey-type crystal is produced (data not shown; see also Margossian and Cohen, 1973). Correspondingly, when TnC is added to preformed double-diamond crystals, no evidence of additional density (TnC binding) is detected (data not shown). These results suggest that the carboxyl-terminal portion of TnT is responsible for the contacts at the acute vertex of the large diamond, most likely through a TnT/TnT association. On this basis, the TnT amino-terminal region would extend into the arms of the mesh. As the amino terminus of TnT spans the head-to-tail overlap of tropomyosin molecules in a filament (White et al., 1987), this joint must lie roughly midway along the arm of the mesh. (Note that the TnT polarity determined from these experiments is opposite that proposed by Carr et al., 1988.)

To extend these observations, a comparison of co-crystals containing different TnT isoforms was carried out. For this purpose, bovine cardiac TnT (TnT284), which has 27 more amino acids near the amino terminus than TnT from rabbit skeletal muscle (TnT259), was used (Leszyk et al., 1987). Structural differences between the double-diamond co-crystals from these two isoforms were examined using the technique of cryoelectron microscopy, which allows the preservation of structural features in unstained specimens embedded in vitreous ice. The electron micrographs of these frozen hydrated double diamonds are remarkably clear (Fig. 2 *A*). Note that the density of the filaments is relatively uniform in these images in contrast to images of negatively stained co-crystals, which show bright stain-excluding nodes at the diamond vertices (Cohen et al., 1972; Carr et al., 1988). A similar finding characterized a comparison of tropomyosin Bailey crystals in negative stain and vitreous ice and is due to the selective enhancement of high protein density by negative stain (Cabral-Lilly et al., 1991; see also Xie et al., 1994). In both co-crystals, TnT appears to be in contact with tropomyosin along its entire length. Fig. 2, *B* and *C*, show maps of a single unit cell for the cardiac and skeletal muscle TnT co-crystals produced by averaging structure factors from several images of each co-crystal type. The overall crystal packing, including the unit cell dimensions and symmetry of this projection, are the same for co-crystals of both TnT isoforms.

Distinctive features in this crystal view were determined from difference maps of the averaged images (Fig. 2, *D* and *E*). The major finding from the maps is that cardiac muscle TnT284 appears to extend from the acute vertex farther into the arm of the mesh beyond the tropomyosin filament joint

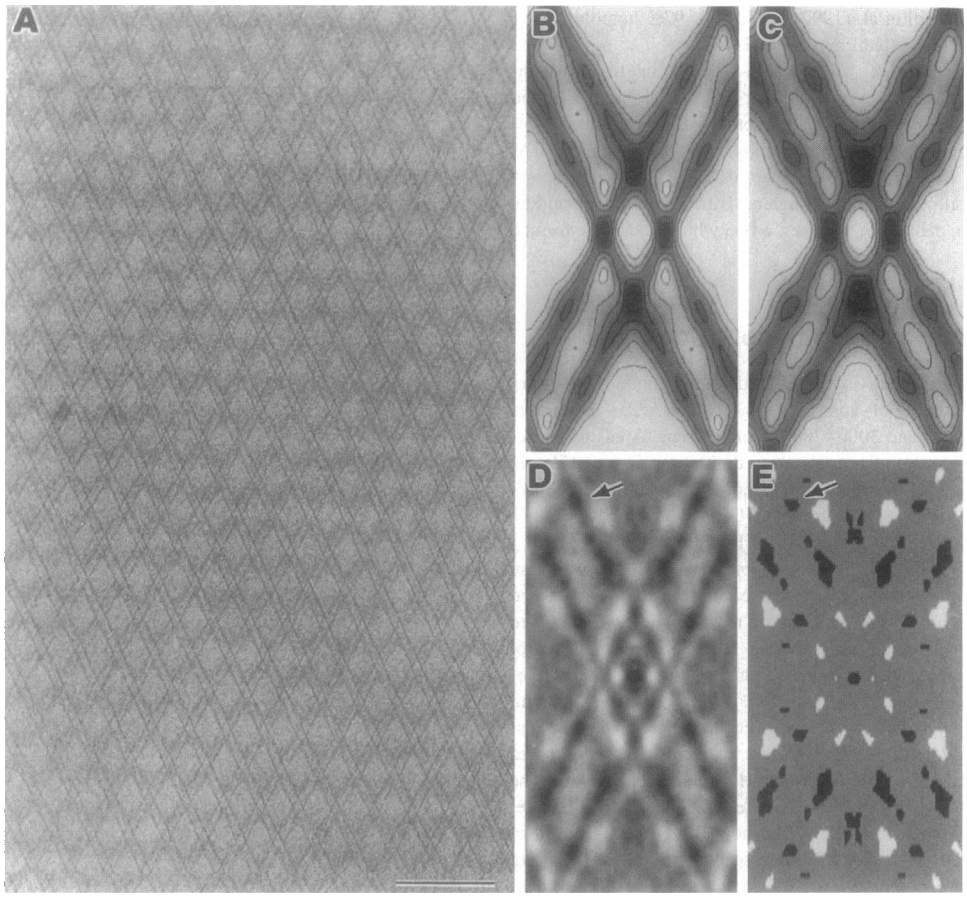

FIGURE 2 Unstained frozen-hydrated double-diamond crystals. Protein appears black; ice is gray or white. (*A*) Electron micrograph of a tropomyosin-TnT284 co-crystal preserved in vitreous ice. Bar, 100 nm. (*B–E*) Density maps of tropomyosin-TnT284 and tropomyosin-TnT259 crystals at 20 Å resolution. The average maps are displayed in *B* of 11 tropomyosin-TnT284 co-crystals and in *C* of 7 tropomyosin-TnT259 crystals. Contour levels equally spaced at 1/5 the total density are superimposed over the gray scale maps. (*D*) Difference map computed by subtracting the map in *C* from the map *B*. Gray areas represent regions in which the two groups are similar. Dark regions in the difference map correspond to additional protein present in the cardiac average whereas white regions correspond to a deficiency of protein in the cardiac average relative to the skeletal average. The statistical significance of differences between the two averages was determined using the Student's *t*-test and is indicated graphically in *E*. Regions of the difference map (*D*) for which there is not a statistical difference (at the 95% confidence level) are displayed in gray in *E*. Regions of protein in *B* that do not correspond to protein in *C* are shown in black in *E*. Regions of protein in *C* that do not correspond to protein in *B* are shown in white. The statistically significant dark area that we point to in *D* and *E* supports a protein density present in the longer cardiac TnT that is absent in the shorter skeletal TnT, located at the end of the TnT molecule farthest from the vertex. This position is where we would expect to find additional protein based on sequence information. Other statistically significant regions are also present (*E*). Most of these lie along the conserved region of the TnT molecule, and we attribute these not to conformational differences in the TnT isoforms but rather to differences in the signal-to-noise ratio in the averaged images. These averages were filtered at 20 Å. However, the cardiac average (*B*) is composed of 11 images, 50% more than the 7 images used for the skeletal average (*C*). The result is that the TnT molecule appears wider and less dense in *C* than it does in *B*. (This is apparent in the difference image (*D*); 1) the white line that includes the statistically significant white spot of *E* would suggest that density is present in *C* that is not present in *B* and 2) the dark line running along the TnT would suggest that the density of cardiac TnT is greater than that of skeletal TnT.) If the two averages had the same signal-to-noise ratio, it would be expected that the region corresponding the conserved portion of TnT would be neutral gray, much the same as the region of ice between filaments.

than does skeletal muscle TnT259 (~180 Å vs. ~160 Å; arrow in Fig. 2 *D*). This difference in length, although close to the resolution of the images, was observed in the processed image of each micrograph and is significant at the 95% confidence level in the difference map (arrow in Fig. 2 *E*). This observation is consistent with the difference in length of the amino-terminal region of the primary sequences of these isoforms (additional residues at the amino terminus of TnT284) as well as with the orientation proposed here for TnT in the lattice. Other statistically significant regions are also present. Most of these lie along the conserved region of the TnT molecule, and we attribute these not to conformational differences in the TnT isoforms but rather to differences in the signal-to-noise ratios in the averaged images (see Legend to Fig. 2).

Because of their appearance in the *c*-axis projection of the negatively stained double diamonds, the tropomyosin filaments were originally thought to be straight with no apparent supercoiling (Cohen et al., 1972). In all crystal forms of native tropomyosin studied so far, however, the filaments are supercoiled with a pitch of approximately 140 Å (Phillips et al., 1986; Whitby et al., 1992; Xie et al., 1994). In the

case of the ice-embedded co-crystals of tropomyosin and TnT, the images also show some evidence of supercoiling distinct from any lattice distortions. (see Fig. 2 *A*). This supercoiling was more obvious when electron micrographs were recorded of samples tilted relative to the electron beam (Fig. 3), indicating that the supercoiling is probably not limited to the *ab* plane (*c*-axis projection). The structure of the tropomyosin-TnT co-crystal appears, however, to be essentially layer-like because of its similarities to the layered structure of a closely related crystal form of tropomyosin induced by spermine (Xie et al., 1994; and see below). Thus, although we cannot yet define the precise nature of the supercoiling in the double-diamond lattice, the extent of bending out of the *ab* plane is probably limited.

Using available information, including the polarity of TnT and its binding sites on tropomyosin, we have developed a schematic three-dimensional model for the tropomyosin-TnT structure (Fig. 4). Of the four orthorhombic space groups ($C222_1$, $C222$, $I222$, and $I2_12_12_1$) that show *cmm* symmetry in projection, we have excluded the body-centered space groups because of the requirement of filament continuity. In considering the other two *C*-centered space groups, we have selected $C222$ for the model as it has the simplest packing arrangement. In building the model, we have been aided by knowledge of the crystal packing in the $C222_1$ spermine-induced tropomyosin crystal structure (Xie et al., 1994). Both crystal forms have the same symmetry in projection (*cmm*) as well as the same diagonal length of the unit cell in projection (~800 Å) although the *b* dimensions of the cells differ. In the case of the spermine-induced crystal, the layer-like structure was deduced by the fact that this diagonal length is close to twice the molecular length, indicating that the *c*-cell dimension must be very small. In the model of the tropomyosin-TnT co-crystal, as in the spermine-induced crystal, pairs of antiparallel tropomyosin filaments lie within a layer of thickness of approximately 45 Å (approximately the sum of the diameters of a tropomyosin plus a TnT molecule). In contrast to the spermine-induced crystal where the layers cross at a small fixed angle, in the tropomyosin-TnT lattice, the *b* dimension is very variable and the layers pack at a number of crossing angles. As the TnT subunits interact face-to-face in the lattice at the acute vertex, they must pivot relative to one another as a result of these varied crossing angles. Thus, as seen in Fig. 1, the lattice appears to be collapsible and forms a paracrystalline fiber when compacted (see also Cohen et al., 1972).

It is of interest to compare the tropomyosin filament interactions in the structures of the double-diamond and Bailey crystal forms (Phillips et al., 1986) as both were produced under similar ionic conditions. In both forms, there are two regions of intermolecular contacts: one near the carboxy terminus and the other approximately 140 Å

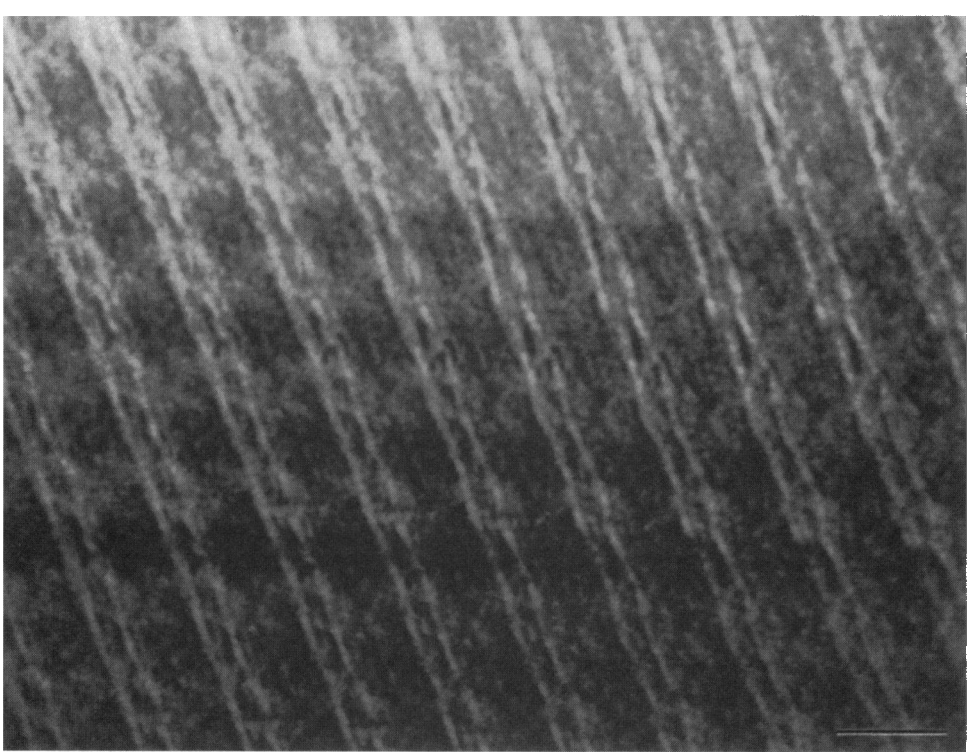

FIGURE 3 Tilted view of a double-diamond mesh in ice. For clarity, the protein is shown as white on a black background. The micrograph was recorded with the electron microscopy grid tilted 20° relative to the electron beam. The tilt axis, calculated from a comparison with a zero-tilt image of the same area, is approximately 35° from the *a* axis. The fast Fourier transform of the digitized image was calculated, high- and low-pass filtered, and then multiplied with a two-dimensional mask with radii of 1.5 pixels centered at each lattice point. An inverse Fourier transform was calculated to produce the noise-filtered image shown. The supercoiling of the tropomyosin filaments can be seen more easily by viewing the figure at an angle from the plane of the paper. Bar, 40 nm.

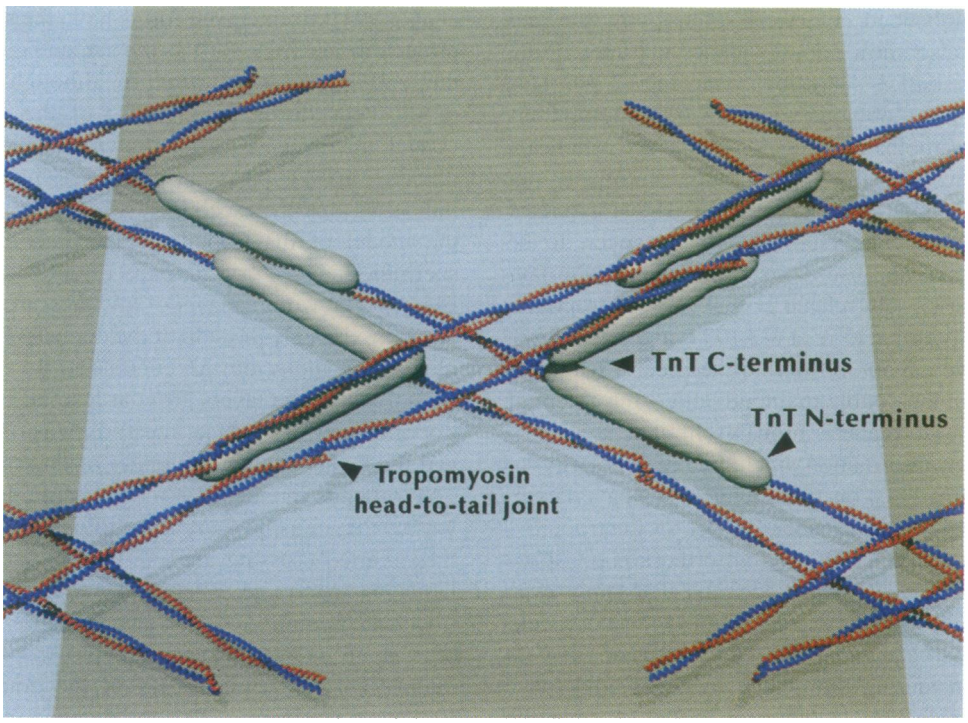

FIGURE 4 A three-dimensional model of the tropomyosin-TnT structure viewed at a tilt angle of ~20° from the *c* axis. The background shows shadows of the tropomyosin-TnT strands (gray) to assist the three-dimensional perspective. The TnT units are modeled as cylindrical rods approximately 180 Å long and 20 Å thick (Flicker et al., 1982) whereas the tropomyosin molecules are modeled on the crystallographic coordinates deposited in the Protein Data Bank (entry pdb2tma.ent; Phillips et al., 1986). The molecules are packed in layered aggregates and a *C*222 cell is assumed so that *cmm* symmetry would be seen in projection. Any supercoiling shown for the tropomyosin filaments is derived from the crystallographic coordinates of the Bailey crystal form. The separation between the filaments is not to scale. The area corresponding to one unit cell depicted in the inset of Fig. 1 *A* is shown with a light background.

from the amino terminus. The former interaction, which occurs at the acute vertex in the double-diamond crystal, is very different from that in the Bailey crystal, in that it involves intermolecular interactions between TnT molecules. The latter interaction, appears, however, to be conserved in both forms. This intermolecular interaction occurs at the obtuse vertex of the double-diamond lattice, which has a crystallographic two-fold as in the Bailey crystal. (We may note that Carr et al. (1988) came to the same conclusion, although they had the opposite polarity for tropomyosin molecules in the double-diamond lattice. This apparent agreement springs from two differences: a reversal in the direction of polarity and a 133 Å shift in the proposed molecular end locations.) Note that in the Bailey crystals this conserved molecular interaction is a very close contact between edges of the coiled coils and is mainly stabilized by electrostatic forces (Phillips et al., 1986). Because of the similar ionic conditions used for crystallization, the close edge contacts may have been conserved in the tropomyosin-TnT co-crystals as well.

Structure-function studies have shown a small quantitative effect of TnT isoform content on calcium sensitivity in isolated muscle fibers and in reconstituted thin filaments (Greaser et al., 1988; Nassar et al., 1991; Schachat et al., 1987; Hatakenaka and Ohtsuki, 1991; Tobacman and Lee, 1987). Other studies have indicated, however, that the TnT amino terminus is not required for thin filament assembly or cooperativity (Pan et al., 1991; Willadsen et al., 1992; Hill et al., 1992). At present, therefore, no clear role has been established for the differences in the amino-terminal structure in the TnT isoforms in the differential regulation of cardiac and skeletal muscle in vivo. Additional studies seem warranted, however, in part because cardiac TnT isoforms are altered in human heart failure (Anderson et al., 1995). Moreover, missense mutations near the alternatively spliced amino-terminal region of TnT are responsible for familial hypertrophic cardiomyopathy in some kindreds (Watkins et al., 1995) and significantly alter actin-myosin interactions (Lin et al., 1996). Contractile function is also affected by hypertrophic-linked mutations occurring in other regions of TnT (Watkins et al., 1996) and by TnT mutations in *Caenorhabditis elegans* (Myers et al., 1996). It is plain that TnT plays a vital role in the sarcomere and that additional structural studies in combination with molecular biology will yield valuable information about this troponin subunit.

We thank Dr. Sudhakara Rao for discussions and comments on the manuscript, Dr. Peter Walian for discussions, Dr. Cameron Owen for work on the difference maps, and Mr. Charles Lee for preparing Fig. 4.

This work was supported by National Institutes of Health grant AR17346 and a grant from the Muscular Dystrophy association (to C. Cohen), National Institutes of Health grant HL-38834 (to L.S. Tobacman), NRSA grant HL-08134 (to J.P. Mehegan), and National Institutes of Health fellowship HL-07682 (to D. Cabral-Lilly).

REFERENCES

Anderson, P. A., A. Grieg, T. M. Mark, N. N. Malouf, A. E. Oakeley, R. M. Ungerleider, P. D. Allen, and B. K. Kay. 1995. Molecular basis of human cardiac troponin T isoforms expressed in the developing, adult, and failing heart. *Circ. Res.* 76:681–686.

Anderson, P. A. W., N. N. Malouf, A. E. Oakley, E. D. Pagani, and P. D. Allen. 1991. Troponin T isoform expression in humans: a comparison among normal and failing heart, fetal heart, and adult and fetal skeletal muscle. *Circ. Res.* 69:1226–1233.

Bandman, E. 1992. Contractile protein isoforms in muscle development. *Dev. Biol.* 154:273–283.

Breitbart, R. E., H. T. Nguyen, R. M. Medford, A. T. Destree, V. Mahdavi, and B. Nadal-Ginard. 1985. Intricate combinatorial patterns of exon splicing generate multiple regulated troponin T isoforms from a single gene. *Cell.* 41:67–82.

Briggs, M. M., and F. Schachat. 1993. Origin of fetal troponin T: developmentally regulated splicing of a new exon in the fast troponin T gene. *Dev. Biol.* 158:503–509.

Cabral-Lilly, D., G. N. Phillips Jr., G. E. Sosinsky, L. Melanson, S. Chacko, and C. Cohen. 1991. Structural studies of tropomyosin by cryoelectron microscopy and x-ray diffraction. *Biophys. J.* 59:805–814.

Carr, H. J., E. J. O'Brien, and E. P. Morris. 1988. Structure of tropomyosin-troponin T co-crystals. *J. Muscle Res. Cell Motil.* 9:384–392.

Cohen, C., D. L. D. Caspar, J. P. Johnson, K. Nauss, S. S. Margossian, and D. A. D. Parry. 1972. Tropomyosin-troponin assembly. *Cold Spring Harbor Symp. Quant. Biol.* 37:287–297.

Cooper, T. A., and C. P. Ordahl. 1985. A single cardiac troponin T gene generates embryonic and adult isoforms via developmentally regulated alternate splicing. *J. Biol. Chem.* 260:11140–11148.

Dahiya, R., C. A. Butters, and L. S. Tobacman. 1994. Equilibrium linkage analysis of cardiac thin filament assembly: implications for the regulation of muscle contraction. *J. Biol. Chem.* 269:29457–29461.

Ebashi, S., and M. Endo. 1968. Calcium ion and muscle contraction. *Prog. Biophys. Mol. Biol.* 18:123–183.

Flicker, P. F., G. N. Phillips Jr., and C. Cohen. 1982. Troponin and its interactions with tropomyosin, an electron microscope study. *J. Mol. Biol.* 162:495–501.

Gahlmann, R., A. B. Troutt, R. P. Wade, P. Gunning, and L. Kedes. 1987. Alternative splicing generates variants in important functional domains of human slow skeletal troponin T. *J. Biol. Chem.* 262:16122–16126.

Greaser, M. L., and J. Gergely. 1973. Purification and properties of the components of troponin. *J. Biol. Chem.* 248:2125–2133.

Greaser, M. L., R. L. Moss, and P. J. Reiser. 1988. Variations in contractile properties of rabbit single muscle fibers in relation to troponin T isoforms and myosin light chains. *J. Physiol.* 406:85–98.

Grieg, A., Y. Hirschberg, P. A. Anderson, C. Hainsworth, N. N. Malouf, A. E. Oakeley, and B. K. Kay. 1994. Molecular basis of cardiac troponin T isoform heterogeneity in rabbit heart. *Circ. Res.* 74:41–47.

Hatakenaka, M., and I. Ohtsuki. 1991. Replacement of three troponin components with cardiac troponin components within single glycerinated skeletal muscle fibers. *Biochem. Biophys. Res. Commun.* 181: 1022–1027.

Henderson, R., J. M. Baldwin, K. H. Downing, J. Lepault, and F. Zemlin. 1986. Structure of purple membrane from *Halobacterium halobium*: recording, measurement and evaluation of electron micrographs at 3.5A resolution. *Ultramicroscopy.* 19:147–178.

Hill, L. E., J. P. Mehegan, C. A. Butters, and L. S. Tobacman. 1992. Analysis of troponin-tropomyosin binding to actin. Troponin does not promote interactions between tropomyosin molecules. *J. Biol. Chem.* 267:16106–16113.

Ishii, Y., and S. S. Lehrer. 1991. Two-site attachment of troponin to pyrene-labeled tropomyosin. *J. Biol. Chem.* 266:6894–6903.

Jin, J. P., and J. J. Lin. 1989. Isolation and characterization of cDNA clones encoding embryonic and adult isoforms of rat cardiac troponin T. *J. Biol. Chem.* 264:14471–14477.

Katus, H. A., S. Looser, K. Hallermayer, A. Remppis, T. Scheffold, A. Borgya, U. Essig, and U. Geuss 1992. Development and in vitro characterization of a new immunoassay of cardiac troponin T. *Clin. Chem.* 38:386–393.

Leszyk, J., R. Dumaswala, J. D. Potter, N. B. Gusev, A. D. Verin, L. S. Tobacman, and J. H. Collins. 1987. Bovine cardiac troponin T: amino acid sequences of the two isoforms. *Biochemistry.* 26:7035–7042.

Lin, D., A. Bobkova, E. Homsher, and L. S. Tobacman. 1996. Altered cardiac troponin T in vitro function in the presence of a mutation implicated in familial hypertrophic cardiomyopathy. *J. Clin. Invest.* 97:2842–2846.

Mair, J., F. Dienstl, and B. Puschendorf. 1992. Cardiac troponin T in the diagnosis of myocardial injury. *Crit. Rev. Clin. Lab. Sci.* 29:31–57.

Mak, A. S., K. Golosinska, and L. B. Smillie 1983. Induction of nonpolymerizable tropomyosin binding to F-actin by troponin and its components. *J. Biol. Chem.* 258:14330–14334.

Mak, A. S., and L. B. Smillie. 1981. Structural interpretation of the two-site binding of troponin on the muscle thin filament. *J. Mol. Biol.* 149: 541–550.

Margossian, S. S., and C. Cohen. 1973. Troponin subunit interactions. *J. Mol. Biol.* 81:409–413.

Mesnard, L., F. Samson, I. Espinasse, J. Durand, J.-Y. Neveux, and J.-J. Mercadier. 1993. Molecular cloning and developmental expression of human cardiac troponin T. *FEBS Lett.* 328:139–144.

Myers, C. D., G. Phuay-Yee, T. S. Allen, E. A. Bucher, and T. Bogaert. 1996. Developmental genetic analysis of troponin T mutations in striated and nonstriated muscle cells of *Caenorhabditis elegans*. *J. Cell Biol.* 132:1061–1077.

Nassar, R., N. N. Malouf, M. B. Kelly, A. E. Oakeley, and P. A. W. Anderson. 1991. Force-pCa relationship and troponin T isoforms in rabbit myocardium. *Circ. Res.* 69:1470–1475.

Pan, B.-S., A. M. Gordon, and J. D. Potter. 1991. Deletion of the first 45 NH_2-terminal residues of rabbit skeletal troponin T strengthens binding of troponin to immobilized tropomyosin. *J. Biol. Chem.* 266: 12432–12438.

Pearlstone, J. R., M. R. Carpenter, and L. B. Smillie. 1986. Amino acid sequence of rabbit cardiac troponin T. *J. Biol. Chem.* 261:16795–16810.

Pearlstone, J. R., P. Johnson, M. R. Carpenter, and L. B. Smillie. 1977. Primary structure of rabbit skeletal muscle troponin T: sequence determination of the NH_2-terminal fragment CB3 and the complete sequence of TnT. *J. Biol. Chem.* 252:983–989.

Phillips, G. N. Jr., J. P. Fillers, and C. Cohen. 1986. Tropomyosin structure and muscle regulation. *J. Mol. Biol.* 192:111–131.

Phillips, G. N. Jr., E. E. Lattman, P. Cummins, K. Y. Lee, and C. Cohen. 1979. Crystal structure and molecular interactions of tropomyosin. *Nature (Lond.).* 278:413–417.

Schachat, F. H., M. S. Diamond, and P. W. Brandt. 1987. Effect of different troponin T-tropomyosin combinations on thin filament activation. *J. Mol. Biol.* 198:551–554.

Schaertl, S., S. S. Lehrer, and M. A. Geeves. 1995. Separation and characterization of the two functional regions of troponin involved in muscle thin filament regulation. *Biochemistry.* 34:15890–15894.

Smillie, L. B., K. Golosinska, and F. C. Reinach. 1988. Sequences of complete cDNAs encoding four variants of chicken skeletal muscle troponin T. *J. Biol. Chem.* 263:18816–18820.

Tobacman, L. S., and R. Lee. 1987. Isolation and functional comparison of bovine cardiac troponin T isoforms. *J. Biol. Chem.* 262:4059–4064.

Trachtenberg, S., D. J. DeRosier, and R. M. Macnab. 1987. Three-dimensional structure of the complex flagellar filament of *Rhizobium lupini* and its relation to the structure of the plain filament. *J. Mol. Biol.* 195:603–620.

Watkins, H., W. J. McKenna, L. Thierfelder, H. J. Suk, R. Anan, A. O'Donaghue, P. Spirito, A. Matsumori, C. S. Moravec, J. G. Seidman, and C. E. Seidman. 1995. Mutations in genes for cardiac troponin T and alpha-tropomyosin in hypertrophic cardiomyopathy. *N. Engl. J. Med.* 332:1058–1064.

Watkins, H., C. E. Seidman, J. G. Seidman, H. S. Feng, and H. L. Sweeney. 1996. Expression and functional assessment of a truncated cardiac troponin T that causes hypertrophic cardiomyopathy: evidence for a dominant negative action. *J. Clin. Invest.* 98:2456–2461.

Whitby, F. G., H. Kent, F. Stewart, M. Stewart, X. Xie, V. Hatch, C. Cohen, and G. N. Phillips Jr. 1992. Structure of tropomyosin at 9 angstroms resolution. *J. Mol. Biol.* 227:441–452.

White, S. P., C. Cohen, and G. N. Phillips Jr. 1987. Structure of co-crystals of tropomyosin and troponin. *Nature (Lond.).* 325:826–828.

Wilkinson, J. M., A. J. Moir, and M. D. Waterfield. 1984. The expression of multiple forms of troponin T in chicken-fast-skeletal muscle may result from differential splicing of a single gene. *Eur. J. Biochem.* 143:47–56.

Willadsen, K. A., C. A. Butters, L. E. Hill, and L. S. Tobacman. 1992. Effects of the amino-terminal regions of tropomyosin and troponin T on thin filament assembly. *J. Biol. Chem.* 267:23746–23752.

Xie, X., S. Rao, P. Walian, V. Hatch, G. N. Phillips Jr., and C. Cohen. 1994. Coiled-coil packing in spermine-induced tropomyosin crystals: a comparative study of three forms. *J. Mol. Biol.* 236:1212–1226.